Diffusiophoresis at the macro-scale

C. Mauger, R. Volk, N. Machicoane, M. Bourgoin, C. Cottin-Bizonne, C. Ybert, F. Raynal

Diffusiophoresis at the macro-scale

C. Mauger,[1] R. Volk,[2] N. Machicoane,[2] M. Bourgoin,[3,2] C. Cottin-Bizonne,[4] C. Ybert,[4] and F. Raynal[1]

[1]*LMFA, CNRS and Université de Lyon, École Centrale Lyon, INSA de Lyon and Université Lyon 1, 69134 Écully CEDEX, France*
[2]*Laboratoire de Physique, ENS de Lyon, CNRS and Université de Lyon, 69364 Lyon CEDEX 07, France*
[3]*LEGI, CNRS, Université Joseph Fourier, Grenoble INP, 38041 Grenoble CEDEX 9, France*
[4]*Institut Lumière Matière, CNRS and Université de Lyon, Université Lyon 1, F-69622 Villeurbanne CEDEX, France*

Diffusiophoresis, a ubiquitous phenomenon which induces particle transport whenever solute gradients are present, was recently put forward in the context of microsystems and shown to strongly impact colloidal transport (from patterning to mixing) at such scales. In the present work, we show experimentally that this nanoscale-rooted mechanism can actually induce changes in the *macro-scale mixing* of colloids by chaotic advection. Rather than the usual decay of standard deviation of concentration, which is a global parameter, we use different multi-scale tools available for chaotic flows or intermittent turbulent mixing, like concentration spectra, or second and fourth moments of probability density functions of scalar gradients. Not only those tools can be used in open flows (when the mean concentration is not constant), but also they allow for a scale by scale analysis. Strikingly, diffusiophoresis is shown to affect all scales, although more particularly the smallest one, resulting in a change of scalar intermittency and in an unusual scale bridging spanning more than 7 orders of magnitude. Quantifying the averaged impact of diffusiophoresis on the macro-scale mixing, we finally explain why the effects observed can be made consistent with the introduction of an effective Péclet number.

I. INTRODUCTION

Diffusiophoresis is responsible for transport of large colloidal particles under the action of solutes [1, 2]. In the case of electrolyte (salt) gradients, as will be considered in the following, it involves two mechanisms, both connected to the presence of the nanometric electrical double layer on the surface of the colloid [1]: the first is purely mechanical and can be explained as a consequence of the existence of gradients of excess of osmotic pressure inside the double layer, while the second is related to electrophoresis of the particles under the electric field induced by the difference in mobility of positive and negative ions of the salt. Interestingly, both contributions lead to an additional transport term for the colloids of the same type, proportional to $\nabla \log S$, where $S(\mathbf{x}, t)$ is the concentration in salt [1] at position $\mathbf{x}$ and time t; the total contribution is called the diffusiophoretic velocity, denoted $\mathbf{v}_{\rm dp}$ (equation 3). The equations of motion are thus given by

$$\frac{\partial S}{\partial t} + \nabla \cdot S\mathbf{v} = D_s \nabla^2 S, \tag{1}$$

$$\frac{\partial C}{\partial t} + \nabla \cdot C(\mathbf{v} + \mathbf{v}_{\rm dp}) = D_c \nabla^2 C, \tag{2}$$

$$\mathbf{v}_{\rm dp} = D_{\rm dp} \nabla \log S, \tag{3}$$

where $C(\mathbf{x}, t)$ is the concentration in colloids, $\mathbf{v}(\mathbf{x}, t)$ is the advecting velocity field, and D_c and D_s are the diffusion coefficients of colloids and salt respectively; $D_{\rm dp}$ is called the diffusiophoretic diffusivity. This set of equations is only valid if $\mathbf{v}$ is negligibly modified by the velocity of the colloids (one way coupling), *i.e.* if the colloidal concentration is not too large; this is the case here. From equation 2, it is clear that colloidal concentration is coupled to that of salt via the diffusiophoretic drift velocity (equation 2), while the salt evolves freely during the process (equation 1). Although the colloids are transported by the total velocity field $\mathbf{v} + \mathbf{v}_{\rm dp}$ (equation 2), diffusiophoresis in laminar mixing can not be seen as a consequence of a large scale effect through a large ratio of velocity amplitudes $V_{\rm dp}/V$, since it remains lower than 1% during the whole experiment (see equation 12 and discussion in paragraph III C); rather, it is related to compressible effects through the diffusiophoretic velocity which is not divergence-free, as recently shown numerically [3]. Thus it has similarities with preferential concentration of inertial particles in turbulent flows [4, 5].

In a recent article, Deseigne *et al.*[6] have studied how diffusiophoresis affects chaotic mixing in a micro-mixer (the so-called staggered herringbone mixer [7], 200 μm wide and 115 μm high). Using only a global characterization —the normalized standard deviation of concentration, a classical tool in mixing studies— they evidenced a diffusiophoretic effect that was interpreted in terms of effective diffusivity (or effective Péclet number). Although constituting a proof of concept, diffusiophoresis was there acting at microns scales which admittedly remains a natural (and small) scale for phoretic transport. Therefore the question of the robustness of this effect on mixing remained largely opened. In particular, one may wonder whether diffusiophoretic effects may extend to chaotic mixing at the macro-scale: will it

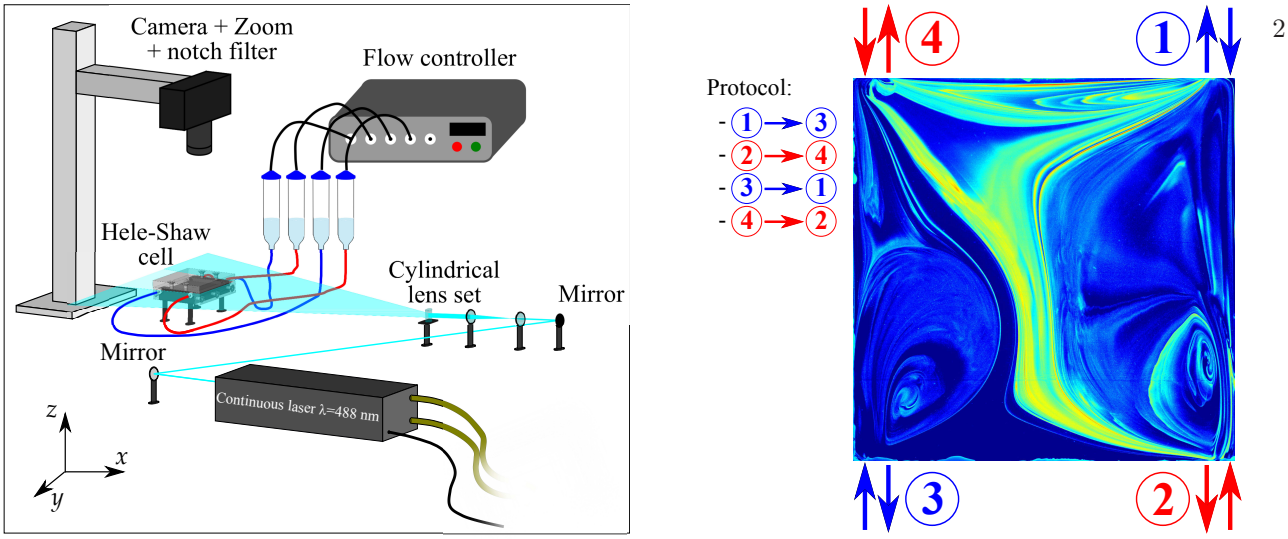

(a) (b)

Figure 1: (a) Scheme of the experimental setup; the square Hele-Shaw cell ($L = 50\,\text{mm}$) lies horizontally in the xy plane. (b) Time-periodic mixing protocol: (i) → (j) indicates that at this step the fluid is pushed at (i) and pumped at (j) during a lapse of time $T/4$, with T the period of the flow-field. The figure displays the instantaneous patterns of a typical concentration field (colloids without salt). A movie showing the type of concentration patterns observed during the whole mixing process is also provided as supplemental material [16].

be able to spread over all length scales or will it remain ineffectively confined at nano-to-micro small scales? This amounts to investigate the possibility of scale-to-scale couplings: while chaotic advection alone affects all scales of a scalar field from the large scale of the macro-container down to the smallest scalar length scale where diffusion is the most effective [8–15], what happens when coupling with diffusiophoresis, whose mechanism applies at the nanoscale? In addition to the very existence of the effect, the quantification of its global impact on mixing also needs to be further investigated. Indeed, as recently discussed theoretically [3], diffusiophoresis is actually related to compressible effects that contain a much richer phenomenology than effective diffusivity concepts: the consistence of such effective approaches thus remains open.

In order to answer those questions we study diffusiophoresis in such a chaotic mixer at the *macro-scale*, that is, with dimensions of the experiment escaping the ones of microsystems by 2 to 3 orders of magnitudes (up to 5 cm global scale). In addition, rather than the usual decay of standard deviation of concentration, which is a global parameter, we apply a set of refined characterizing analyses, using different multi-scale tools available from the turbulence community, like concentration spectra (section III A), or second and fourth moments of probability density functions (PDF) of scalar gradients (section III B). These more elaborated tools allow us to perform a scale by scale analysis and thus study how all scales of scalar field can be affected by diffusiophoresis. Finally, after evidencing the propagation of diffusiophoretic effects up to the macro-scale, we discuss the introduction of an effective Péclet number approach to quantify it.

II. DESCRIPTION OF THE EXPERIMENT

A. Experimental set up

Mixing takes place in a horizontal square Hele-Shaw cell of side $L = 50\,\text{mm}$ and height $h = 4\,\text{mm}$, supplied by 4 inlets/outlets (figure 1). Each inlet/outlet is pressure-driven using a flow controller (Fluigent, MFCS). At $t = 0$, a quantity of 0.2 ml of a fluorescent solution (either dye or colloidal suspension) is introduced via inlet 1 inside the Hele-Shaw cell initially filled with water (or salted water, see later) using a syringe pump. The four inlets/outlets are then pressurized under 100 mbar, and fluid motion is carried out by successive pressurization and depressurization of the inlets/outlets: a movie showing the mixing process is provided as supplemental material [16]. Successive deformations of the scalar field are characterized by Planar Laser-Induced Fluorescence (PLIF): a continuous laser (Coherent Genesis MX SLM-Series, $\lambda = 488 \pm 3$ nm) coupled to a cylindrical lens forms a laser sheet with a typical thickness of the order of the cell height, so that the whole volume of the cell is illuminated. The choice of using a thick laser sheet rather than a thin one localized at the mid-height of the cell will be discussed at the end of section II C.

The fluorescence signal is recorded with a 14-bit camera (Nikon D700, 4200 px × 2800 px) whose lens (zoom 105 mm) is equipped with a band reject filter (notch 488 ± 12 nm) corresponding to the laser wavelength. ISO sensitivity is set to lowest value in order to avoid noise, aperture to highest (i.e. $f/3.5$), with a shutter speed of 12.5 ms. Image resolution in both horizontal directions (x or y) is about $19\,\mu\mathrm{m.px}^{-1}$, while the depth of field is of the order of 1 mm. Calibration for different fluorescent species and different concentrations showed a linear behavior between the light intensity and the concentration of the species throughout the range studied.

B. Flow-rate and mixing

Chaotic advection is enabled via the time-periodic protocol illustrated in Figure 1*b*, with four stages of same duration $T/4$ each. When considering chaos efficiency in such a Hele-Shaw cell, the important parameter is the dimensionless pulse volume α

$$\alpha = \frac{qT}{L^2\,h}\,, \tag{4}$$

where q is the flow-rate; α represents the volume of fluid displaced during one period compared to the volume of the chamber [17, 18]. For this particular mixing protocol, a global chaos (no visible regular region) is obtained for $\alpha \geq 1.2$ [17, 19]. Because large values of α would imply rather high flow-rates (hence large Reynolds numbers) or large periods T (hence very long mixing time [20]), we chose to consider the smallest value of interest $\alpha = 1.2$.

In a Hele-Shaw cell, the Reynolds number Re_h is classically based on the height h of the cell, *i.e.*, with a typical velocity $q/(hL)$ and kinematic viscosity ν,

$$\mathrm{Re}_h = \frac{q}{L\nu}. \tag{5}$$

Note that the Reynolds number inside the pipes connected to the inlets/outlets,

$$\mathrm{Re}_{pipes} = \frac{4q}{\pi\,d\,\nu}, \tag{6}$$

with $d = 1\,\mathrm{mm}$ the diameter of the pipes, is quite higher. Because in the present case $\mathrm{Re}_{pipes} = 64\ \mathrm{Re}_h$, we set $\mathrm{Re}_h = 1$ in order to avoid a large Reynolds number in the pipe and hence non reproducible experiments. This corresponds to a flow-rate $q = 50\,\mu\mathrm{L\,s}^{-1}$, and, providing $\alpha = 1.2$, we obtain the smallest period $T = 120\,\mathrm{s}$; this is the period we used. Note that with those parameters, the flow is totally laminar and deterministic, as can also be appreciated on the movie [16]. As a consequence, the advecting velocity $\mathbf{v}$ in equations 1 and 2 is *identical* for all the cases considered here (except for the short initial transient stratification, discussed in annexe A for cases with salt). Each of the experiments in this article was carried out twice, so as to avoid any error: because of its repeatability, the results obtained (Taylor scale, effective Péclet numbers, *etc.*) were identical for both runs.

Since we are interested in mixing, the relevant parameter is the Péclet number, that measures the relative effect of advection compared to diffusion; because in a Hele-Shaw flow with chaotic advection, mixing essentially takes place in the horizontal direction [21], we will consider thereafter the Péclet number based on the width L of the cell,

$$\mathrm{Pe} = \frac{q}{hD}, \tag{7}$$

with D the diffusion coefficient of the species considered.

C. Diffusiophoresis

For this study we used colloids of diameter 200 nm (FluoSpheres, LifeTechnologies F8811), marked with a yellow-green fluorophore (wavelength 505/515 nm); in order to induce diffusiophoresis, we also used a 20 mM solution of salt (LiCl). LiCl was shown in microfluidic experiments to have a stronger diffusiophoretic effect compared to other salts [2]. These same microfluidic experiments revealed that diffusiophoretic drift of this class of particles in a gradient of LiCl induces a motion of the colloids from low to high salt concentration regions. In the following, we discuss the interplay between mixing and diffusiophoretic drift by considering three different cases:

- *reference*: the colloids are injected inside pure water;

Species	Diffusion coefficient [$m^2.\ s^{-1}$]	Péclet number
Colloids	$2.\ 10^{-12}$	$6.\ 10^6$
Dextran	$3.6\ 10^{-11}$	$3.\ 10^5$
Fluorescein	$4.\ 10^{-10}$	$3.\ 10^4$
Salt (LiCl)	$1.4\ 10^{-9}$	$9.\ 10^3$

Table I: Species used, diffusion coefficients and corresponding Péclet numbers

- *salt-in*: the salt is introduced together with the colloids inside pure water; in this configuration diffusiophoresis showed hypo-diffusion (delayed mixing) in the staggered herringbone micro-mixer [6].
- *salt-out*: the colloids are injected inside salted water; in this configuration diffusiophoresis showed hyper-diffusion (enhanced mixing) in the staggered herringbone micro-mixer.

For a more systematic exploration of Péclet number effects on the mixing process, other species (molecular) have also been considered, namely fluorescein isothiocyanate (FITC) and fluorescent dextran 70 000 MW (LifeTechnologies D1823). For such molecular species diffusiophoresis is not expected to play a role. They will be used to characterize the efficiency of mixing as a function of the Péclet number (at fixed geometry and flow forcing) in order to quantify possible deviations from the trend potentially induced by diffusiophoresis in the case of colloids. The diffusion coefficients and corresponding Péclet numbers for all species used in the experiment are available in table I: the variation amplitude of the Péclet number is more than two orders of magnitude.

Note from equation 1 that, whereas the concentration in colloids is coupled to that of salt, the concentration in salt S freely evolves during the experiment. Thus the salt is fully mixed for $t \geq L^2\, h/(2q) \ln(\mathrm{Pe}_s)$ [22, 23], with $\mathrm{Pe}_s = q/(h\, D_s)$ the Péclet number for salt, that is $t \sim 900\,\mathrm{s}$ with our parameters. After that time diffusiophoresis no more affects colloids (although the global effect is still visible, *i.e.* mixing enhancement or reduction [3]). In what follows we will restrict to times where diffusiophoresis is fully effective.

Note finally that, because of buoyancy effects, the salt tends to rapidly stratify inside the cell (see appendix A). Hence, although they are almost isodense with water, the colloids tend to go from mid-height where they are injected towards the bottom of the cell because of a vertical diffusiophoresis, following this salt gradient (appendix A). This "settling" of colloids, only visible when salt is present and which goes against the effective buoyancy (more salted water in the bottom being denser than colloids, that are isodense in pure water), already reveals a first macroscopic effect of diffusiophoresis. Because it became difficult to follow the colloids at long times using a very thin laser sheet (they would eventually disappear below the sheet), and because the flow is quasi 2D, we chose to illuminate the whole cell. This kind of height-averaging can result in a loss of signal at very large wavenumbers, especially in the salt-in case; however the coupling of the parabolic flow with diffusion also leads to some vertical homogenization of the scalar field in a Hele-Shaw cell, although mixing is much more rapid in the horizontal direction because of chaotic advection [21]. Indeed, we will see that we are still able to quantify a clear effect in terms of effective Péclet number.

III. RESULTS

When measuring mixing efficiency, the quantity commonly used is the rate of decay of standard deviation of the concentration $C_{std}(t) = < (C - < C >)^2 >^{1/2}$, or the non-dimensional standard deviation $\sigma(t) = C_{std}(t)/C_{std}(t=0)$ [24], where $< . >$ stands for the spatial average. Indeed, without diffusiophoresis, the rate of decay of $C_{std}(t)$ is related to the presence of high scalar gradients through the equation

$$\frac{d\, C_{std}^2}{dt} = -2D < (\nabla C)^2 > . \tag{8}$$

Note that diffusion operates at all scales, but is much more efficient at small scale where the gradients are more intense. In the following, as commonly done by fluid mechanicists, the quantity $\frac{1}{2}(C - < C >)^2 = \frac{1}{2} C_{std}^2(t)$ is referred to as *scalar energy*, by analogy with the kinetic energy.

Above all, chaotic advection involves a large range of scalar scales from the macro-scale of the experiment down to the smallest length scale involved, while diffusiophoresis involves a mechanism at the nano-scale. Thus such a *global* parameter as σ is not enough to explore this typically *multi-scale coupled* problem. For instance, does diffusiophoresis strongly dissipate scalar energy at a very small scale, or else interact with the flow so as to dissipate more smoothly at all length scales involved? In addition, let us note that even for global characterization, σ would not be an appropriate parameter here anyway since the flow is an open flow (marked particles go in and outside the chamber through the inlet/outlets during the periodic mixing protocol, *i.e.* $< C > (t) \neq cst$).

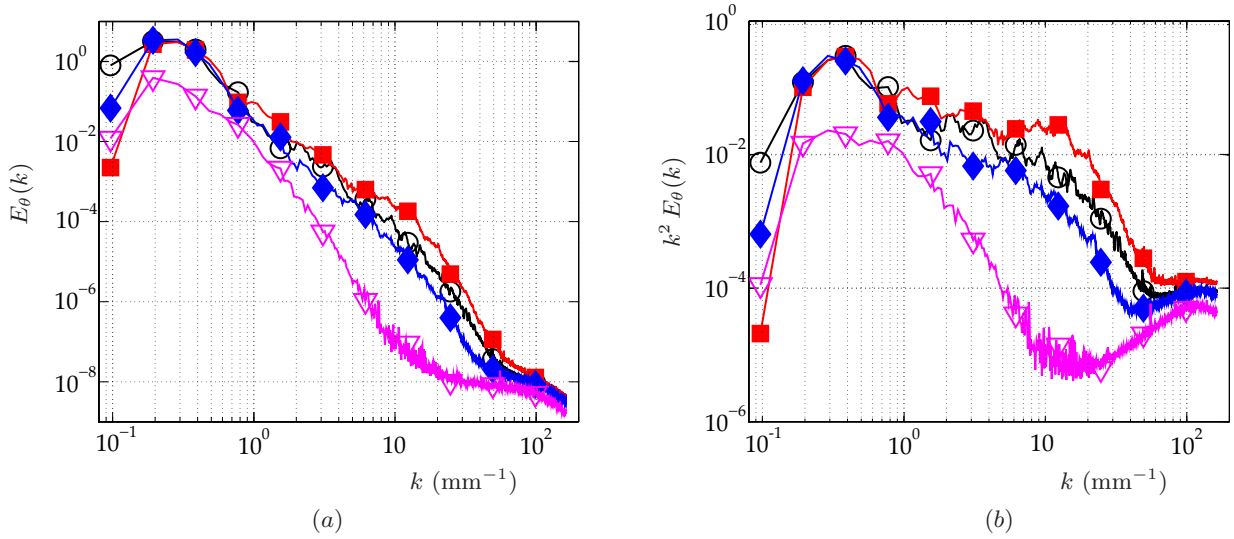

(a) (b)

Figure 2: (a) Instantaneous spectra of scalar energy (time $t = 160\,$s); (b) Instantaneous dissipation spectra, same time. Open symbols stand for cases without salt. ○: reference case (no salt); ■: salt-in; ♦: salt-out; ▽: fluorescein. The scalar energy spectrum and dissipation spectrum for fluorescein have been divided by 10.

In order to investigate the multi-scale properties of the scalar field, we used different tools more commonly available from fluid mechanics community, and adapted for such a multi-scale process:

- *the scalar energy spectrum* $E_\theta(k)$ is a usual means in chaotic advection studies [11, 25–28]; it quantifies the scalar energy contained at a given wavenumber $k = 2\pi/\ell$, where ℓ can be seen as the physical scale at which the scalar energy is calculated, *i.e.* the typical width of a scalar structure; it is linked to the *global* scalar energy through the relation $\frac{1}{2}C_{std}^2 = \int_0^\infty E_\theta(k)\,dk$.
- *PDFs of scalar gradients* (more widely encountered in turbulent mixing [29, 30], see also [11, 31]); while *global* dissipation of scalar energy is linked to scalar gradients through equation 8, such a parameter does allow to investigate whether dissipation occurs mainly with gradients quite close to the mean gradient (as can be seen for instance with a gaussian distribution), or else is related to very intense *local* gradients, in which case we refer to *spatial* intermittency. In the present study, each image (corresponding to a given time t) allows to obtain $\mathcal{O}(6.\,10^6)$ scalar gradient values in each direction, further used to compute one PDF.

A. Scalar energy spectra

Instantaneous scalar energy spectra $E_\theta(k)$ are calculated from individual concentration fields at a given time by using the 2D-Fourier-transform $\hat{\theta}(k_x, k_y, t)$ of the reduced scalar field $\theta(x, y, t) = (C(x, y, t) - < C(x, y, t) >)/C_{std}(t)$; in order to reduce aliasing due to non-periodic boundary conditions, a window-Hanning method was used. The 1D isotropic spectrum was then obtained by averaging over each $k = (k_x^2 + k_y^2)^{1/2}$.

Figure 2(a) shows typical instantaneous scalar energy spectra for the three configurations, reference case (without salt), salt-in and salt-out. Clearly, the small amount of salt visibly impacts the whole spectrum, although small scalar scales are more affected than large scales (as for diffusion effects). In the salt-in case (solid squares), the spectrum extends further towards large wavenumbers (small scales) than the reference spectrum. This kind of behavior would also be observed if considering the concentration spectrum of a species that diffuses less than the colloid we used. Indeed, since diffusion is directly related to scalar dissipation through equation 8, a smaller diffusion coefficient D (therefore a larger Péclet number) implies that the final scalar dissipation occurs with larger scalar gradients, *i.e.* at an even smaller lengthscale: the spectrum would also be shifted towards larger wavenumbers. In the salt-out case, the effect is reversed, with a shift towards smaller wavenumbers. As a comparison and in order to show the influence of a much smaller Péclet number, we have also plotted in the figure the spectrum of fluorescein, although it was divided by 10 for clarity.

The effect is even clearer when looking at the term $k^2\,E_\theta(k)$, proportional to the scale by scale dissipation budget (figure 2(b)): diffusiophoresis obviously affects all lengthscales ranging roughly from the centimeter ($k \geq 0.8\,\text{mm}^{-1}$) down to the smallest scales resolved. Quite remarkably, this demonstrates that diffusiophoresis can indeed influence

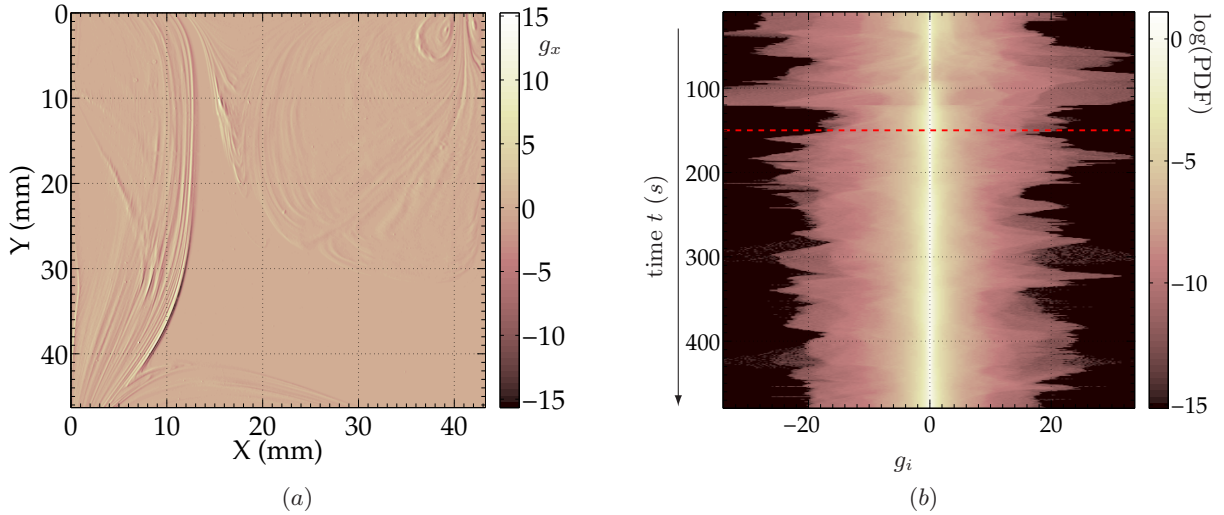

Figure 3: Reference case with colloids (no salt); (a): instantaneous reduced gradient x-component, $g_x = (G_x - < G_x >)/G_{x|std}$, where $G_x = \partial C/\partial x$ (at time $t = 293\,\mathrm{s}$). (b): time evolution of log(PDF) of all reduced gradient components g_i, where g_i stands for g_x and g_y ($\mathrm{PDF}(g_i) = 1/2[\mathrm{PDF}(g_x) + \mathrm{PDF}(g_y)]$). The dotted line at $t = 150\,\mathrm{s}$ corresponds to the moment when PDFs become reasonably periodic in time, so that time-averaging is conceivable.

mixing processes way beyond its nanometric roots or its micrometric classical influence. Combined with chaotic mixing multi-scale process, it can spread over more than 7 orders of magnitude in length scales and affect the global system.

However one should note that the previous diagnosis relies on an instantaneous analysis: while the flow is time periodic, the large scale patterns –and therefore the large scales of the associated spectra– also vary with time, as can be appreciated on the movie included as supplemental material [16]. Indeed the effect is not always as pronounced as in figure 2, at some (rare) moments of the periodic cycle the effect is even reversed, as also found in our numerical simulations [3]. Since most of the scalar energy is contained in larger scales (hence in small wavenumbers k), it is therefore not easy to obtain a time-averaged parameter from the concentration spectra that would accurately measure a global effect of salt. As observed in the spectra, small scalar scales are more affected by diffusiophoresis: we therefore propose to investigate the concentration gradients, so as to obtain quantitative comparison that considers a global effect over time.

B. Concentration gradients

In order to obtain the concentration gradients $\mathbf{G} = \nabla C$, a given image of the concentration field (corresponding to a given time t) is first filtered using a Gaussian kernel to get rid of potential noise: filtering over two pixels ($\approx 40\,\mu m$) is fairly enough to obtain the gradients with great accuracy. Then we measure the two components of the concentration gradients, $G_x = \partial C/\partial x$ and $G_y = \partial C/\partial y$ at each point of the image. For component x (respectively y), we calculate the mean gradient component over the whole image $< G_x >$ (respectively $< G_y >$), and also the standard deviation $G_{x|std} =< (G_x - < G_x >)^2 >^{1/2}$ (respectively $G_{y|std}$). In the following, we investigate the reduced gradient component g_i:

$$g_i = (G_i - < G_i >)/G_{i|std}\,, \tag{9}$$

where i stands for x and y. In figure 3a we plot the reduced gradient x-component g_x at a given time ($t = 293\,\mathrm{s}$, which corresponds to 2 1/4 periods of the flow-field) in the reference case (no salt). Note the very large amplitude range from -15 to 15, indicating that scalar gradient *spatial* fluctuations are not Gaussian (events of large amplitude are more likely to happen than in a Gaussian case, which is usually referred to as spatial intermittency). This is reminiscent of the intense and intermittent gradient fronts produced by the mixing process, that are well captured when computing this quantity. This results in stretched PDFs of scalar gradient as it will be shown later in figure 4b. While g_x and g_y have equivalent statistics, it is interesting to consider the mean statistics that are even better converged: figure 3b shows the PDF of the normalized gradient component g_i, $\mathrm{PDF}(g_i) = 1/2[\mathrm{PDF}(g_x) + \mathrm{PDF}(g_y)]$, as a function of time (one PDF every second). In the experiment, after a transient mixing phase where the initial spot of marked dye begins to spread in the whole domain (roughly one period of the flow-field T), the global patterns

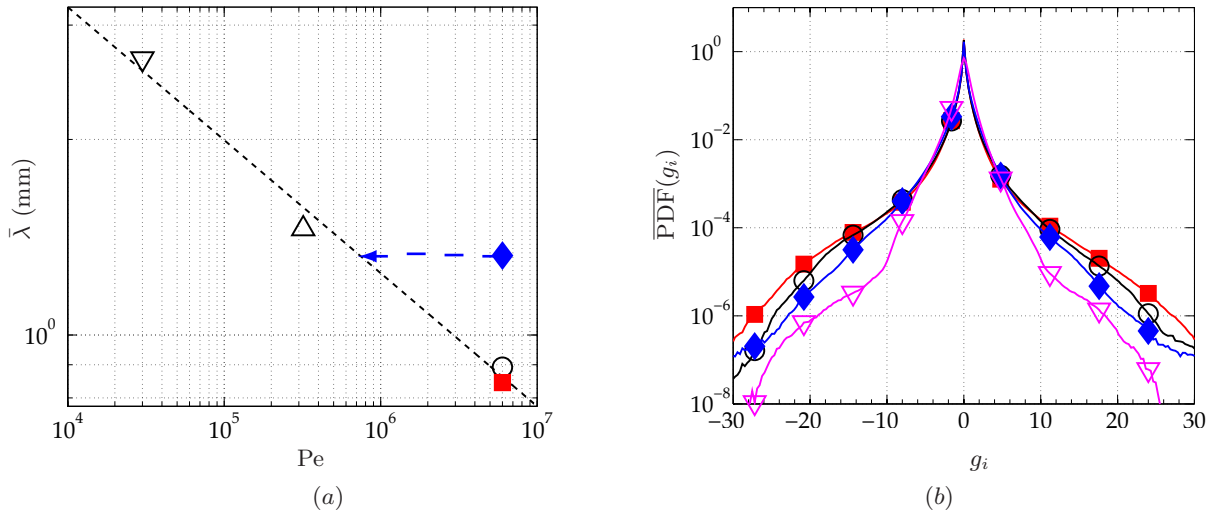

Figure 4: (a) Taylor scale of scalar gradients, $\bar{\lambda}$, defined as the time-average of $\lambda = 2\,C_{std}/\sqrt{G^2_{x|std} + G^2_{y|std}}$. The arrow indicates the effective Péclet number defined as the corresponding reference Péclet number that leads to the same value of $\bar{\lambda}$. (b): time averaged PDF of reduced concentration gradients g_i, $\overline{\mathrm{PDF}}(g_i)$. Open symbols stand for cases without salt. ○: reference case (no salt); ■: salt-in; ♦: salt-out; ▽: fluorescein. For sake of clarity dextran is omitted in this plot.

become almost periodic with time (with period of the flow-field), *i.e.* have a similar shape each period. This is also visible in figure 3b for times $t \geq 150\,\mathrm{s}$ (shown with a dotted line in the figure), where the PDFs have a similar *shape* every period $T = 120\,\mathrm{s}$, with abrupt events occurring typically every $T/4$, *i.e.* associated with a different phase of the periodic protocol (figure 1b). In the sequel we consider time-averaged data, denoted by an over-bar, averaged on the interval of time $150\,\mathrm{s} \leq t \leq 470\,\mathrm{s}$. We can now compare cases with or without salt.

For each image (*i.e.* for each time), we define the Taylor length scale associated with scalar gradients as $\lambda = 2\,C_{std}/\sqrt{G^2_{x|std} + G^2_{y|std}}$, and consider its time-average value $\bar{\lambda}$ (averaged over $150\,\mathrm{s} \leq t \leq 470\,\mathrm{s}$) in figure 4$a$. When mixing without salt is considered (open symbols, corresponding to cases without any diffusiophoretic effect), $\bar{\lambda}$ roughly follows a decaying power-law with Péclet number. In the salt-out case, $\bar{\lambda}$ is clearly greater than in the reference case. We can define an effective Péclet number as the corresponding reference Péclet number that leads to the same value of $\bar{\lambda}$ (as suggested by the arrow); we obtain a much smaller effective Péclet number than for the reference case, $\mathrm{Pe}^{salt-out}_{eff} \approx 8.\,10^5$, that has to be compared to $\mathrm{Pe} \sim 6.\,10^6$. In the salt-in case, the effect is less clear; this may be due to the very definition of this quantity, only based on std values of concentration and gradients (second order statistics), which are not as sensitive to the intermittency of the scalar field as higher order moments. In order to check this hypothesis we plot in figure 4b the time-average of the instantaneous $\mathrm{PDF}(g_i)$, denoted by $\overline{\mathrm{PDF}}(g_i)$, with or without salt; for sake of clarity we omitted the plot for dextran. When comparing first the cases without salt (open symbols, corresponding to colloids and fluorescein mixing statistics), we recover the usual enhancement of small scale scalar intermittency with increasing Pe [29]: the wings of the PDF are much higher, suggesting that events of large amplitude are more likely to happen. When salt is added (closed symbols), once again we recover (with a time-averaged plot rather than the instantaneous ones of figure 2) that the salt-out configuration corresponds globally to a smaller effective Péclet number. In the salt-in case, we observe the effect of a larger Péclet number for strong values of gradients, although the plot is hardly distinguishable from the reference case for $-15 \leq |g_i| \leq 15$ (which explains indeed why the two corresponding points are so close in figure 4a). Because the effect of intermittency is more visible on the fourth moment than on the second one, we propose to calculate the flatness of this time-averaged distribution. Indeed, the quantity $g_i^4\ \overline{\mathrm{PDF}}(g_i)$, plotted in figure 5$a$, shows a much pronounced effect in the salt-in case. This is even more visible when considering the flatness F of the distribution shown in figure 5b: while the flatness in the cases without salt remarkably follows an increasing power-law with the Péclet number, the salt-out case rather corresponds to an effective Péclet number roughly the same as the one found with the second moment of gradients ($\bar{\lambda}$), $\mathrm{Pe}^{salt-out}_{eff} \approx 10^6$ ($\mathrm{Pe}^{salt-out}_{eff}/\mathrm{Pe} \sim 1/6$), while the salt-in case leads to $\mathrm{Pe}^{salt-in}_{eff} \approx 2.\,10^7$ ($\mathrm{Pe}^{salt-in}_{eff}/\mathrm{Pe} \sim 3$).

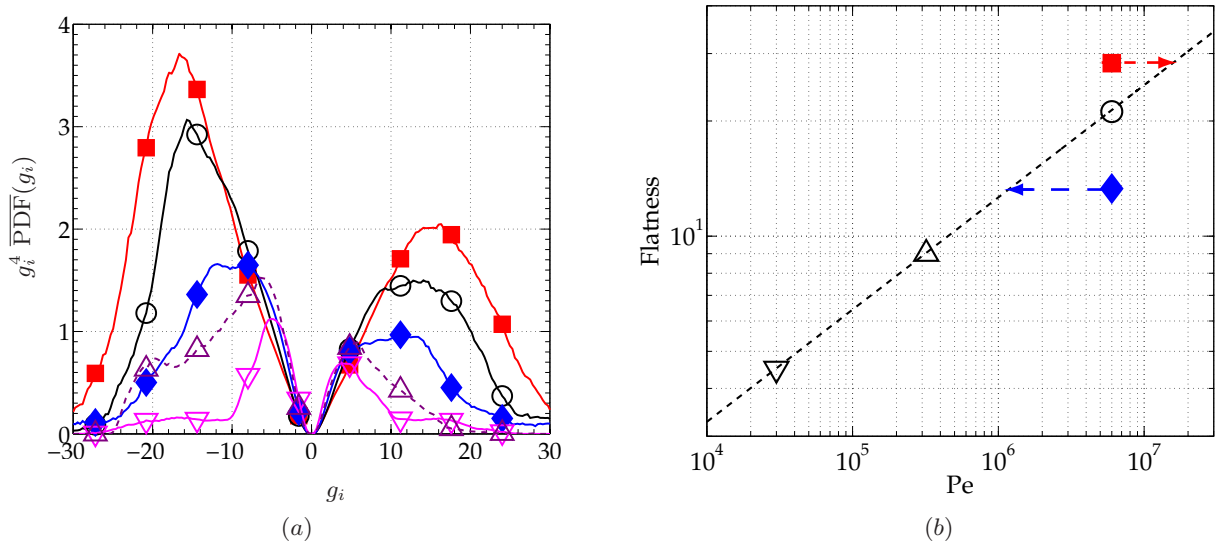

(a) (b)

Figure 5: (a): $g_i^4\ \overline{\mathrm{PDF}}(g_i)$, where $\overline{\mathrm{PDF}}(g_i)$ is the time-averaged PDF of g_i for the cases under study. (b): flatness of the time averaged PDF, $F = (\int g_i^4\ \overline{\mathrm{PDF}}(g_i)\ dg_i)/(\int g_i^2\ \overline{\mathrm{PDF}}(g_i)\ dg_i)^2$, with $\|g_i\| \leq 30$). The arrows indicate the effective Péclet numbers defined as the corresponding reference Péclet numbers that lead to the same flatness. Open symbols stand for cases without salt. ○: reference case (no salt); ■: salt-in; ♦: salt-out; △: dextran; ▽: fluorescein.

C. Discussion

Overall, our experimental results evidence that nano-scale diffusiophoresis is able to affect large particles mixing at the macro-scale. More precisely, using a multi-scale approach to interpret our experimental results, we have shown that diffusiophoresis affects all scales of the scalar field, although small scales are even more affected: because the same could be said for diffusion, the effect of diffusiophoresis on the scalar field has some similarities with diffusive effects. This provides a clue as to why it is useful and meaningful to introduce an effective Péclet number when considering the long time effects, and to try to quantify the combined effects of diffusiophoresis and diffusion with that effective approach.

We now compare quantitatively our results on the global influence of diffusiophoresis at the macro-scale with the one obtained at the micro-scale with the herringbone micro-mixer by Deseigne *et al.* [6]. Although the flow-field in the herringbone micro-mixer is stationary and 3-dimensional, it may however be compared favorably with what can be expected in a two-dimensional time-periodic flow: indeed, Stroock & McGraw [32] proposed an analytical model in which the cross-section of the channel is treated as a lid-driven cavity flow; they showed that this model was able to reproduce the advection patterns that were observed experimentally in their flow, whose dimensions are about the same as in Deseigne *et al.* (roughly 200 μm wide, 100 μm high). Here, because of the spatial periodicity in the axial direction, the corresponding coordinate plays the role of time.

When considering the experiment in the staggered herringbone micro-mixer, the effect is rather more important than in the present case. In their case they obtained $\mathrm{Pe}_{\mathit{eff}}^{\mathit{salt-out}}/\mathrm{Pe} \sim 1/40$ and $\mathrm{Pe}_{\mathit{eff}}^{\mathit{salt-in}}/\mathrm{Pe} \sim 20$. Note however that in both experiments the effect is twice more important in the salt-out than in the salt-in case, *i.e.* $\mathrm{Pe}^2 = 2\,\mathrm{Pe}_{\mathit{eff}}^{\mathit{salt-out}}\,\mathrm{Pe}_{\mathit{eff}}^{\mathit{salt-in}}$.

There are different explanations for the shift between both experiments. Above all, remember that the present flow is an open flow ($<C>(t) \neq cst$), while the other one is not ($<C>(t) = cst$ in all planes perpendicular to the axial direction): colloids and salt go in and out of the cell, which could make the effect less important because of dilution. Indeed, in a perfect Stokes flow without diffusion, a fluid particle that enters into one of the pipes during one stage of the periodic flow-field would not move in the following stage, and finally come back to its original position in the chamber at the end of the next stage [19]. In the pipes, because of diffusion and small inertial effects, particles may slightly move and sometimes remain in the pipes when the flow is reversed.

This may also come from the kind of "height-averaging" when illuminating the whole cell, that could make the higher gradients slightly underestimated.

Another reason could be related to the value of the Péclet number in the micro-mixer, that has to be based on the cross-sectional velocity rather than on the axial velocity for a legitimate comparison. With their model, Stroock & McGraw could also estimate the magnitude of the velocity u_{cross} in the cross-sectional flow relative to the axial velocity U: taking $u_{\mathrm{cross}} \sim 0.1\,U$, with a channel width $w = 200\,\mu$m and $U = 8.6$ mm/s, we obtain a colloidal Péclet

number $\mathrm{Pe} \sim 9.\,10^4$, that is, much smaller than in the present article ($6.\,10^6$).

In order to check if the difference in Péclet number could induce some of the shift observed, we propose to estimate the order of magnitude of the diffusiophoretic term: from equation 3, we obtain

$$V_{\mathrm{dp}} \sim \frac{D_{\mathrm{dp}}}{\ell_s} \ , \tag{10}$$

with ℓ_s the typical length-scale of salt gradients, resulting from a competition of contraction by the chaotic flow-field and diffusion. Because the salt is not coupled to the colloids, it verifies [22]:

$$\ell_s \sim \frac{L}{\sqrt{\mathrm{Pe}_s}} \ , \tag{11}$$

where Pe_s is the salt Péclet number. Finally, from equations 10 and 11, we obtain:

$$\frac{V_{\mathrm{dp}}}{V} \sim \frac{D_{\mathrm{dp}}}{\sqrt{D_c\, D_s}}\, \mathrm{Pe}^{-1/2} ; \tag{12}$$

this order of magnitude is in accordance with what we found numerically [3] (with the parameters used for our numerical study we obtain from equation 12 that $V_{\mathrm{dp}}/V \sim 4.\,10^{-3}$ while we found numerically $7.\,10^{-3}$). Note that with the colloids used for the experiment we have $D_{\mathrm{dp}} = 2.9\,10^{-10}\,\mathrm{m}^2.\,\mathrm{s}^{-1}$, so that we obtain from equation 12 an even smaller ratio $V_{\mathrm{dp}}/V \sim 2.2\,10^{-3}$. Since the colloids are transported by the total velocity field $\mathbf{v}+\mathbf{v}_{\mathrm{dp}}$ (equation 2), and since the relative effect of diffusiophoresis decreases with the Péclet number (equation 12), this could also explain part of the shift (the relative effect is 8 times larger in the micro-mixer because of the difference in Péclet number). Note however that equation 12 can not be used to measure directly the difference in effective Péclet numbers: indeed, the effective Péclet number does not result from diffusiophoresis effects only, but also from diffusion effects, whose relative strength compared to transport by the velocity field also decreases with the Péclet number from its very definition.

Finally, let us note that although useful and convenient, this effective Péclet approach is only approximate, and is best grounded for the salt-out configuration where mixing is enhanced. In that respect, it is quite remarkable that the effective Péclet for the salt-out case is indeed robust against the experimental observable used, either the Taylor scale of scalar gradients or the flatness of the distribution.

As a matter of fact, strictly speaking diffusiophoresis is not a diffusive effect. Indeed we have clearly shown in a recent numerical work [3] that a more general framework relates to the flow compressibility, and that a global parameter like the standard deviation of concentration σ could increase at small times in the salt-in case, whereas diffusion can only cause σ to decrease with time (equation 8). This is especially the case for the salt-in case where diffusiophoresis acts *against* diffusion, effectively inducing an "anti-diffusion" that reinforces gradients at early times. This is the reason why salt-in characteristics do not show up as easily in averaged quantities, and require going to the fourth order moment of the distribution of gradients, rather than the Taylor scale associated to the second moment.

IV. SUMMARY

In this article we have studied experimentally the effects of diffusiophoresis on chaotic mixing of colloidal particles in a Hele-shaw cell at the macro-scale. We have compared three configurations, one without salt (reference), one with salt with the colloids (salt-in), and a third one where the salt is in the buffer (salt-out). Rather than the usual decay of standard deviation of concentration, which is a global parameter, we have used different multi-scale tools like concentration spectra, second and fourth moments of the PDFs of scalar gradients, that allow for a scale by scale analysis; those tools are also available in open flows, when marked particles can go in and out the domain under study.

Using scalar spectra, we have shown qualitatively that diffusiophoresis affects all scalar scales. This demonstrates that this mechanism at the nano-scale has an effect at the centimetric scale, *i.e.* 7 orders of magnitude larger. Because the smallest scalar scales are more affected, this results in a change of spatial intermittency of the scalar: using second and fourth moments of the PDFs of scalar gradients, we have been able to quantify globally the impact of diffusiophoresis on mixing at the macro-scale. Although diffusiophoresis is clearly related to compressibility, we have explained how the combined effects of diffusiophoresis and diffusion are consistent *when averaging in time* with the introduction of an effective Péclet number: the salt-in configuration corresponds to a larger effective Péclet number than the reference case, and the opposite for the salt-out configuration. Because this results from a time-averaged study, and not from an instantaneous diagnostic, this demonstrates that diffusiophoresis, whose mechanism applies at the nanoscale, has a quantitative effect on mixing at the macro-scale.

Acknowledgments

This collaborative work was supported by the LABEX iMUST (ANR-10-LABX-0064) of Université de Lyon, within the program "Investissements d'Avenir" (ANR-11-IDEX-0007) operated by the French National Research Agency (ANR).

Appendix A: Stratification of salt and associated migration of colloids

As seen in section II C, salt induces a rapid stratification of the flow. This can be explained using characteristic time scales: the typical buoyancy time scale τ_A for a less dense particle at the bottom to reach the top of the cell is given by the Archimedes' principle, $\Delta\rho\, g = \rho h/\tau_A^2$, where g is gravity, ρ is density, and $\Delta\rho = \rho\beta\Delta C$ is linked to the difference of salt concentration ΔC through the expansion coefficient β. With $\beta = 2.4\,10^{-2}\mathrm{M}^{-1}$ for LiCl [33] and $\Delta C = 20\,\mathrm{mM}$, we obtain $\tau_A \simeq 0.92\,\mathrm{s}$. While the viscous time scale τ_v that tends to dump the vertical velocity is $\tau_v = h^2/\nu = 16\,\mathrm{s}$, and the diffusion time scale τ_d that tends to erase concentration gradients in the vertical direction by diffusion is $\tau_d = h^2/D_s \sim 3\,\mathrm{h}$, the Rayleigh number of the flow, $\mathrm{Ra} = \tau_v\,\tau_d/\tau_A^2 = \beta\Delta C\, g\, h^3/(\nu\, D_s) \sim 216\,000$, is way higher than the critical value. However, unlike Rayleigh-Bénard convection, we have no source of buoyancy in this experiment, so that the vertical movement stops (typically after time τ_v) when all heavy fluid has fallen at the bottom while the lighter fluid is at the top: the fluid is rapidly stratified inside the cell.

Once this stable stratification is set, a vertical gradient of salt appears, that can settle a colloid movement because of diffusiophoresis. Following equation 3, the vertical diffusiophoretic velocity, $\mathbf{v}_{\mathrm{dp}} \sim D_{\mathrm{dp}}\,\nabla S/S \sim D_{\mathrm{dp}}/h$. The typical time scale $\tau_{\mathrm{dp}}^{vert}$ associated to vertical diffusiophoresis is the time taken for a particle to go from half-depth where it is injected down to the bottom, hence $\tau_{\mathrm{dp}}^{vert} \sim h^2/(2D_{\mathrm{dp}}) \sim 8\,\mathrm{h}$. Although this is rather long, we could observe, when using a very thin laser sheet (300μm-thick) that colloids tended to disappear below the sheet at large times. This is why we chose to illuminate the whole cell.

[1] J. L. Anderson. Colloid transport by interfacial forces. *Annu. Rev. Fluid. Mech.*, 21, 1989.
[2] B. Abécassis, C. Cottin-Bizonne, C. Ybert, A. Ajdari, and L. Bocquet. Osmotic manipulation of particles for microfluidic applications. *New Journal of Physics*, 11(7):075022, 2009.
[3] R. Volk, C. Mauger, M. Bourgoin, C. Cottin-Bizonne, C. Ybert, and F. Raynal. Chaotic mixing in effective compressible flows. *Phys. Rev. E*, 90:013027, Jul 2014.
[4] M. Maxey. The Gravitational Settling Of Aerosol-Particles In Homogeneous Turbulence And Random Flow-Fields. *Journal of Fluid Mechanics*, 174:441–465, 1987.
[5] R. A. Shaw. Particle-Turbulence interactions in atmospheric clouds. *Annual Review of Fluid Mechanics*, 35:183–227, 2003.
[6] J. Deseigne, C. Cottin-Bizonne, A. D. Stroock, L. Bocquet, and C. Ybert. How a "pinch of salt" can tune chaotic mixing of colloidal suspensions. *Soft Matter*, 10:4795–4799, 2014.
[7] A. D. Stroock, S. K. W. Dertinger, A. Ajdari, I. Mezic, H. A. Stone, and G. M. Whitesides. Chaotic Mixer for Microchannels. *Science*, 295:647–651, 2002.
[8] H. Aref. Stirring by chaotic advection. *J. Fluid Mech.*, 143:1–21, 1984.
[9] J.M. Ottino. *The Kinematics of Mixing: Stretching, Chaos and Transport.* Cambridge University Press, New-York, 1989.
[10] V. Rom-Kedar, A. Leonard, and S. Wiggins. An analytical study of the transport, mixing and chaos in an unsteady vortical flow. *J. Fluid Mech.*, 214:347–394, 1990.
[11] R. T. Pierrehumbert. Tracer microstructure in the large-eddy dominated regime. *Chaos, Solitons & Fractals*, 4(6):1091–1110, 1994.
[12] S. Cerbelli, A. Adrover, and M. Giona. Enhanced diffusion regimes in bounded chaotic flows. *PHys. Let. A*, 312:355–362, 2003.
[13] E. Gouillart, J-L Thiffeault, and M. D. Finn. Topological mixing with ghost rods. *Phys. Rev. E*, 73:036311, Mar 2006.
[14] D. R. Lester, G. Metcalfe, and M. G. Trefry. Is chaotic advection inherent to porous media flow? *Phys. Rev. Lett.*, 111:174101, Oct 2013.
[15] O. Gorodetskyi, M.F.M. Speetjens, and P.D. Anderson. Eigenmode analysis of advective-diffusive transport by the compact mapping method. *European Journal of Mechanics - B/Fluids*, 49, Part A:1 – 11, 2015.
[16] See supplemental material at [CollRefFin-crop.avi] , movie showing the type of concentration patterns observed in the time-periodic flow-field ($T = 120\,\mathrm{s}$), here in the reference case (colloids without salt).
[17] F. Raynal, A. Beuf, F. Plaza, J. Scott, Ph. Carrière, M. Cabrera, J.-P. Cloarec, and E. Souteyrand. Towards better DNA chip hybridization using chaotic advection. *Phys. Fluids*, 19:017112, 2007.
[18] A. Beuf, J. N. Gence, Ph. Carrière, and F. Raynal. Chaotic mixing efficiency in different geometries of hele-shaw cells. *Int. J. Heat Mass Transfer*, 53:684–693, 2010.

[19] F. Raynal, F. Plaza, A. Beuf, Ph. Carrière, E. Souteyrand, J.-R. Martin, J.-P. Cloarec, and M. Cabrera. Study of a chaotic mixing system for DNA chip hybridization chambers. *Phys. Fluids*, 16(9):L63–L66, 2004.
[20] F. Raynal and J.-N. Gence. Efficient stirring in planar, time-periodic laminar flows. *Chem. Eng. Science*, 50(4):631–640, 1995.
[21] F. Raynal, A. Beuf, and Ph. Carrière. Numerical modeling of DNA-chip hybridization with chaotic advection. *Biomicrofluidics*, 7(3):034107, 2013.
[22] F. Raynal and J.-N. Gence. Energy saving in chaotic laminar mixing. *Int. J. Heat Mass Transfer*, 40(14):3267–3273, 1997.
[23] E. Villermaux, A. D. Stroock, and H. A. Stone. Bridging kinematics and concentration content in a chaotic micromixer. *Physical Review E*, 77(1):015301, 2008.
[24] E. L. Paul, V. A. Atiemo-obeng, and S. M. Kresta, editors. *Handbook of Industrial Mixing: Science and Practice*. Wiley Interscience, 2003.
[25] B. S. Williams, D. Marteau, and J. P. Gollub. Mixing of a passive scalar in magnetically forced two-dimensional turbulence. *Physics of Fluids (1994-present)*, 9(7):2061–2080, 1997.
[26] V. Toussaint, Ph. Carrière, J. Scott, and J.-N. Gence. Spectral decay of a passive scalar in chaotic mixing. *Phys Fluids*, 12(11):2834–2844, 2000.
[27] M.-C. Jullien, P. Castiglione, and P. Tabeling. Experimental observation of batchelor dispersion of passive tracers. *Phys. Rev. Lett.*, 85:3636–3639, Oct 2000.
[28] P. Meunier and E. Villermaux. The diffusive strip method for scalar mixing in two dimensions. *Journal of Fluid Mechanics*, 662:134–172, 11 2010.
[29] M. Holzer and E. D. Siggia. Turbulent mixing of a passive scalar. *Physics of Fluids*, 6(5):1820–1837, 1994.
[30] Z. Warhaft. Passive scalars in turbulent flows. *Annual Review of Fluid Mechanics*, 32(1):203–240, 2000.
[31] R. T. Pierrehumbert. Lattice models of advection-diffusion. *Chaos*, 10(1):61–74, 2000.
[32] A. D. Stroock and G. J. McGraw. Investigation of the staggered herringbone mixer with a simple analytical model. *Philosophical Transactions of the Royal Society of London A: Mathematical, Physical and Engineering Sciences*, 362(1818):971–986, 2004.
[33] *CRC handbook of chemistry and physics, 92nd ed.* CRC Press, Boca Raton, FL, 2011.